INT. J. NUM. METH. HEAT FLUID FLOW, VOL. 6, NO. 8, 31–52 (1996)

GENERATION OF STABLE THERMAL STRATIFICATION IN A PARTIALLY ENCLOSED SPACE DUE TO A ROOM FIRE

ABDULKARIM H. ABIB AND YOGESH JALURIA

Department of Mechanical & Aerospace Engineering, Rutgers University, New Brunswick, NJ , USA

ABSTRACT

A numerical study of a two-dimensional turbulent flow in a partially open rectangular cavity such as a room is carried out. The turbulent flow is induced by the energy input due to a localized heat source positioned on the floor of the cavity. This flow is of interest in enclosure fires where the flow in the cavity interacts with the environment through the opening or vents. The focus is on the stable, thermal stratification that arises in the room and on the influence of the opening height. A finite-difference method is employed for the solution of the problem, using a low Reynolds number $k-\varepsilon$ turbulence model for the turbulent flow calculations. This model is particularly suitable for flows in which the possibility for relaminarization exists. It was found that, for high Grashof numbers and for relatively small opening heights, particularly for doorway openings, a strong stable thermal stratification is generated within the cavity, with a cooler, essentially uniform, layer underlying a warmer, linearly stratified, upper layer. As a consequence, turbulence is suppressed and the flow in the upper region of the cavity becomes laminar with turbulence confined to locations such as the fire plume above the source and the shear layer at the opening. The penetration distance and the height of the interface are both found to decrease with a reduction in the opening height. The Nusselt number for heat transfer from the source is seen to be affected to a small extent by the opening height. The basic trends are found to agree with those observed in typical compartment fires. Comparisons with results available in the literature on turbulent buoyancy-driven enclosure flows indicate good agreement, lending support to this model and the numerical scheme.

KEY WORDS Stratification Natural convection Room fire Stable stratification Partial enclosure Enclosure

NOMENCLATURE

A = aspect ratio, $A = l/h$
$C_{1\varepsilon}, C_{2\varepsilon}$ = empirical constants in the turbulence model
$C_{3\varepsilon}, C_{\mu}$ = empirical constants in the turbulence model
f_1, f_2, f_{μ} = damping wall functions in the turbulence model
Gr = Grashof number based on the height of the cavity $Gr = g\beta\frac{Q_0}{\kappa}h^3/\nu^2$
g = magnitude of the gravitational acceleration
$\bar{h}$ = Average heat transfer coefficient
h = height of the cavity
h_t = height of the interface
h_0 = height of the opening
H_0 = dimensionless height of the opening, h_0/h
K = dimensionless turbulent kinetic energy
l = length of the cavity
l_e = length of the extended computational domain
l_s = length of heat source
l_t = thickness of the doorway soffit
L_e = dimensionless length of the extended computational domain, $L_e = l_e/h$
L_s = dimensionless length of heat source, $L_s = l_s/h$
L_t = dimensionless thickness of the doorway soffit, $L_t = l_t/h$
$\dot{m}$ = dimensionless mass outflow rate at the opening
$\overline{Nu_s}$ = average Nusselt number over the source, defined in equation (21)
n = normal distance from nearest wall
Pr = Prandtl number, $Pr = \frac{\nu}{\alpha}$
Q_0 = total heat input by the energy source per unit width
Re_n = local Reynolds number, $Re_n = \sqrt{k}n/\nu$
Re_t = local Reynolds number, $Re_t = k^2/\nu\varepsilon$
T = temperature
t = dimensionless time
U,V dimensionless mean velocity components in the X and Y co-ordinate directions, respectively
x = horizontal co-ordinate
x_s = distance between the source and the back wall
X = dimensionless horizontal co-ordinate, x/h
X_s = dimensionless distance between the source and the back wall, $X_s = x_s/h$
y = vertical co-ordinate
Y = dimensionless vertical co-ordinate, y/h
Z_i = dimensionless height of hot-cold interface

Greek

α = thermal diffusivity
β = coefficient of thermal expansion, $\beta = 1/T$ for perfect gas
γ = stratification level
δ_p = dimensionless penetration height of the thermal plume
ε = dimensionless dissipation of turbulent kinetic energy
κ = coefficient of thermal conductivity
ν = kinematic viscosity
ν_e = effective eddy diffusivity, $\nu_e = 1 + \nu_t/\nu$
ν_t = turbulent eddy diffusivity
ρ = density
ΔT_q = characteristic temperature difference, $\Delta T_q = Q_0/\kappa$

0961–5539/96

Received January 1995
Revised January 1996

Δt = dimensionless time step
θ = dimensionless temperature, $\theta = \frac{T-T_\infty}{\Delta T_e}$
ψ = dimensionless stream function
σ_ϵ = turbulent Prandtl numbers for ϵ
σ_t, σ_k = turbulent Prandtl numbers for θ, and K respectively
ζ = dimensionless vorticity

Subscripts
e = effective value of turbulent eddy diffusivity
i = hot-cold interface
s = heat source
w = wall value

INTRODUCTION

Transport processes in partially open enclosures (hereafter referred to as POE) are very different from those in similar completely closed enclosures. They are usually strongly dependent on the nature, size, location and number of openings or vents, as well as on the temperature distribution in the ambient medium. For instance, the effect of venting or entrainment of air on the growth of a fire and on the removal of combustion gases from the enclosure is very important and is well recognized[1,2]. In fact, in a developing fire, venting controls the temperature and heat transfer, thereby influencing the spread of the fire. In a fully developed fire, the rate of inflow of air controls the rate of fuel combustion. On the other hand, the flow in a POE is significantly affected by the ambient medium surrounding the opening, especially, when the ambient is stably stratified[3]. Indeed, these effects include turbulence suppression and relaminarization of the flow in the upper region of the enclosure.

The study of convective flows arising from energy sources located at the bottom in a partially open enclosure is considered. This problem, with either localized or volumetric energy sources and isothermal ambient medium outside the opening, has received considerable attention in the last 35 years[4-10]. However, the effects of thermal stratification have received much less attention despite its importance in enclosure fires. In fact, in room fires, the thermal stratification influence is felt in several ways[11]. At first, it affects the location of the interface (hot-cold interface) between the hot combustion products and the cold inflow at bottom by inhibiting the rise of fire or thermal plume above the heat source. Thus the knowledge of the location of the hot-cold interface becomes very crucial to the detection and control of a fire. Second, when the thermal stratification is stable, it results in a decay of the turbulence and, hence, leads to relaminarization of the flow, see the review by Quintiere[2]. This may then alter the transport processes and distort the simplistic concept of two homogeneous gas layers, which form the basis of the zone modelling analysis of room fires.

The primary objective of the present study is to investigate the interaction between the ambient media and the POE with a localized energy source at the bottom boundary. The study explores the effect of opening height at various Grashof numbers Gr. Furthermore, a comparison is made between this case and the case where the environment surrounding the opening of a POE is stably and thermally stratified owing to the presence of a thermal energy source in an adjacent corridor or a room. The effort is mainly directed at determining the heat transfer rate, mass flow rate, the penetration distance of the fire plume rising above the source, and the turbulence and stratification levels that are generated within the cavity, in order to characterize the resulting penetrative and recirculating flow. This information will be valuable in modelling turbulent flow and mixing in room fires.

ANALYSIS

The problem of interest

A numerical study of the turbulent penetrative and recirculating flow caused by energy input at the bottom boundary of a partially open rectangular cavity of height H and aspect ratio (length to height) A of two, typical of room-size enclosures, is carried out. This flow is of particular interest in the simulation of flows induced by room fires, which was the motivation for this work. A rectangular cavity with an opening is connected to a very long corridor which is initially isothermal as shown in Figure 1. A single doorway opening is examined since the effect of

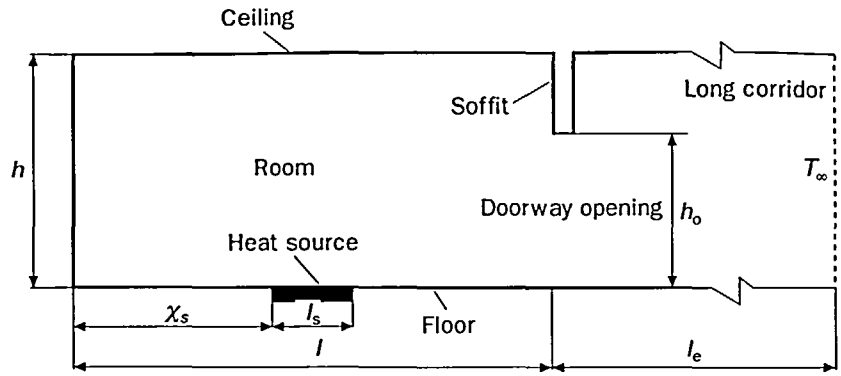

Figure 1 A partially open enclosure heated at the bottom boundary by a localized energy source

multiple openings is less significant than that of the opening size, as far as growth and flashover potential of fire is concerned[12].

For the present study, the energy source is a localized heat source with a constant heat input per unit width, Q_0. The role of thermal radiation in the gases is ignored and the focus is on convective flow and transport since interest lies in regions far from the energy source. This is a reasonable approximation for $Gr < 10^{13}$. However, radiation effects are important near the source and should be included. This work focuses on the basic characteristics of the flow and the effects of the opening. The side walls, the floor and the ceiling are considered to be adiabatic, assuming that these have heated up and are well-insulated.

Governing equations

The governing equations, in dimensionless form, expressing conservation of mass, momentum, energy, and the turbulent kinetic energy and the dissipation rate, for an incompressible Boussinesq fluid, can be written as:

$$U = \frac{\partial \psi}{\partial Y}; \qquad V = -\frac{\partial \psi}{\partial X} \tag{1}$$

$$\frac{\partial^2 \psi}{\partial X^2} + \frac{\partial^2 \psi}{\partial Y^2} = -\zeta \tag{2}$$

$$\frac{\partial \zeta}{\partial t} + \frac{\partial (U\zeta)}{\partial X} + \frac{\partial (V\zeta)}{\partial Y} = \frac{1}{\sqrt{Gr}} \left\{ \frac{\partial}{\partial X} \left(\frac{\partial (\nu_e \zeta)}{\partial X} \right) + \frac{\partial}{\partial Y} \left(\frac{\partial (\nu_e \zeta)}{\partial Y} \right) \right\} + S_\zeta \tag{3}$$

$$\frac{\partial \Theta}{\partial t} + \frac{\partial (U\Theta)}{\partial X} + \frac{\partial (V\Theta)}{\partial Y} = \frac{1}{Pr\sqrt{Gr}} \left\{ \frac{\partial}{\partial X} \left(\nu_{e,\Theta} \frac{\partial \Theta}{\partial X} \right) + \frac{\partial}{\partial Y} \left(\nu_{e,\theta} \frac{\partial \Theta}{\partial Y} \right) \right\} \tag{4}$$

$$\frac{\partial K}{\partial t}+\frac{\partial(UK)}{\partial X}+\frac{\partial(VK)}{\partial Y} = \frac{1}{Pr\sqrt{Gr}}\left\{\frac{\partial}{\partial X}\left(\nu_{e,k}\frac{\partial K}{\partial X}\right)+\frac{\partial}{\partial Y}\left(\nu_{e,k}\frac{\partial K}{\partial Y}\right)\right\} + P + G - \epsilon \tag{5}$$

$$\frac{\partial \epsilon}{\partial t}+\frac{\partial(U\epsilon)}{\partial X}+\frac{\partial(V\epsilon)}{\partial Y} = \frac{1}{Pr\sqrt{Gr}}\left\{\frac{\partial}{\partial X}\left(\nu_{e,\epsilon}\frac{\partial \epsilon}{\partial X}\right)+\frac{\partial}{\partial Y}\left(\nu_{e,\epsilon}\frac{\partial \epsilon}{\partial Y}\right)\right\} + \frac{\epsilon}{K}\{C_{1\epsilon} f_1(P + C_{3\epsilon} G) - C_{2\epsilon} f_2 \epsilon\} \tag{6}$$

where S_ζ is the source term for the mean vorticity equation, given by

$$S_\zeta = \frac{\partial \Theta}{\partial X}+\frac{1}{\sqrt{Gr}}\left\{2\left(\frac{\partial U}{\partial Y}\right)\frac{\partial^2 \nu_e}{\partial X^2}-2\left(\frac{\partial V}{\partial X}\right)\frac{\partial^2 \nu_e}{\partial Y^2} + 4\left(\frac{\partial V}{\partial Y}\right)\frac{\partial^2 \nu_e}{\partial Y \partial X}\right\} \tag{7}$$

and G and P are buoyancy and shear production of the turbulent kinetic energy, defined as

$$G = -\frac{1}{\sqrt{Gr}}\frac{\nu_t^*}{\sigma_t}\frac{\partial \Theta}{\partial Y} \tag{8}$$

$$P = \frac{\nu_t^*}{\sqrt{Gr}}\left\{\left(\frac{\partial U}{\partial Y}+\frac{\partial V}{\partial X}\right)^2+2\left(\frac{\partial U}{\partial X}\right)^2+2\left(\frac{\partial V}{\partial Y}\right)^2\right\} \tag{9}$$

with

$$\nu_t^* = \frac{\nu_t}{\nu} = \sqrt{Gr}\, f_\mu C_\mu \frac{K^2}{\epsilon} \tag{10}$$

Here ν_e, $\nu_{e,\theta}$, $\nu_{e,k}$, and $\nu_{e,\varepsilon}$ are the effective turbulent diffusivities defined as

$$\nu_e = 1 + \nu_t^* ; \qquad \nu_{e,\theta} = 1 + \frac{Pr\,\nu_t^*}{\sigma_t} \tag{11}$$

$$\nu_{e,k} = 1 + \frac{\nu_t^*}{\sigma_k} ; \qquad \nu_{e,\epsilon} = 1 + \frac{\nu_t^*}{\sigma_\epsilon} \tag{12}$$

The damping wall functions f_1, f_2, and f_μ for the modified low-Reynolds ($k-\varepsilon$)-model of Lamb and Bremhorst[13,14] hereafter denoted as MLB, are:

$$
\begin{aligned}
f_1 &= 1 + \left(\frac{0.14}{f_\mu}\right)^3 \\
f_2 &= \left[1 - 0.27\exp\left(-Re_t^2\right)\right]\left[1 - \exp\left(-Re_n\right)\right] \\
f_\mu &= \exp\left\{-\frac{3.4}{(1 + Re_t/50)^2}\right\} \\
Re_t &= \frac{K^2}{\nu\epsilon} \\
Re_n &= \frac{\sqrt{K}n}{\nu}
\end{aligned}
\tag{13}
$$

where n is the normal distance from the nearest wall. The coefficients C_μ, $C_{1\varepsilon}$, $C_{2\varepsilon}$, $C_{3\varepsilon}$, σ_t, σ_k and σ_ε are empirical constants given in Table 1. These constants are recommended by Launder and Spalding[15] except for the constant $C_{3\varepsilon}$ in the buoyancy term of the $\in$-equation, which is suggested by Rodi[16] to be close to 1 in vertical boundary layers and close to 0 in horizontal layers. For the present work $C_{3\varepsilon}$ was adopted from Fraikin *et al.*[17] as $C_{3\varepsilon} = 0.7/C_{1\varepsilon}$. Thus, all the constants are those used in the literature. No variation from these values is employed in this study. All the symbols are defined in the nomenclature.

The governing equations give rise to three dimensionless parameters: the Grashof number Gr, the Prandtl number Pr, and the opening height H_0. Since the fluid considered is air the Prandtl number Pr is set equal to 0.72. The parameters of the problem are then reduced to two, namely, G_r and H_0. The size of the energy source l_s is set equal to $0.2h$ and the source location is taken as the centre of the cavity ($x_s = 0.9h$). Other values for the source size and location are also considered. These results are not reported here since the main focus is on the influence of the opening height and since the basic trends are not strongly affected by a variation in these values.

Initial and boundary conditions

The appropriate initial and boundary conditions for the equations (1)-(6) are given as below. Initially, at $t = 0$, the room and the surrounding ambient are assumed to be isothermal ($\theta = 0$). A laminar flow solution is used to specify the profiles for U, V, ψ, and ζ. In addition, non-zero perturbations in K and ν_t (typically, $K = 10^{-6}$ and $\nu_t^* = \frac{\nu_t}{\nu} = 10$) are used and the energy dissipation rate is computed as $\varepsilon = \sqrt{Gr}C_\mu\frac{K^2}{\nu_t^*}$. The boundary conditions at the solid boundaries (including the floor, the ceiling, the door soffit, and the left side wall) are

$$
U = V = \psi = K = \frac{\partial\epsilon}{\partial \mathrm{n}} = \frac{\partial\Theta}{\partial \mathrm{n}} = 0, \quad \zeta = \zeta_w,
\tag{14}
$$

where n is the direction normal to the boundary. The thermal boundary conditions at the energy source are

$$
\frac{\partial\Theta}{\partial \mathrm{Y}} = \dot{\mathrm{q}}_o'' = \tfrac{1}{L_s}, \quad X_s \le X \le X_s + L_s.
\tag{15}
$$

Table 1 Empirical constants for the $(k-\varepsilon)$-model recommended by Launder and Spalding[15]

C_μ	$C_{1\varepsilon}$	$C_{2\varepsilon}$	$C_{3\varepsilon}$	σ_θ	σ_k	σ_ε
0.09	1.44	1.92	0.7	0.9	1.0	1.3

Finally, at the far-field (X→∞) the boundary conditions are

$$V = \frac{\partial U}{\partial X} = \frac{\partial \psi}{\partial X} = \frac{\partial \zeta}{\partial X} = \frac{\partial K}{\partial X} = \frac{\partial \epsilon}{\partial X} = 0, \quad 0 \le Y \le 1 \tag{16}$$

$$\begin{cases} \Theta = 0 & \text{if } U \le 0, \quad 0 \le Y \le 1 \quad \text{(inflow)} \\ \dfrac{\partial \Theta}{\partial X} = 0 & \text{if } U > 0, \quad 0 \le Y \le 1 \quad \text{(outflow).} \end{cases} \tag{17}$$

NUMERICAL SOLUTION

The statistically averaged equations governing the mean-flow quantities are given in equations (1)-(6). Despite the time averaging, the unsteady terms are kept in the formulation of the governing equations to account for possible unsteadiness in the transport processes. The time averaging is carried out over a time period that is larger than the time scale of turbulence but *smaller than the time scale of the mean motion.*

The governing equations are discretized with the control-volume based finite difference method in stream function vorticity formulation. The advection and diffusion terms are discretized with the power-law scheme[18]. The temporal discretization is executed implicitly. A modified version of the low Reynolds number $k-\varepsilon$ model of Lam and Bremhorst[13,14] is used in the turbulent flow calculations. This model is particularly suitable for flows in which a potential for re-relaminarization exists. The solution for θ, ζ, ψ, K, and ε is obtained by an iterative procedure at each time step. The details of the numerical scheme used are given by Abib[19].

The existence of the boundary layer near the walls requires that a non-uniform grid be used that gives a strong grid refinement along the walls. A hyperbolic grid distribution is employed, with the grid points given by

$$\frac{x_i}{h} = \frac{1}{2}\left\{1 + \frac{\tanh\left[\alpha_1(i/i_{max} - \frac{1}{2})\right]}{\tanh(\alpha_1/2)}\right\} \; i = 0, 1, 2, \ldots, i_{max} \tag{18}$$

$$\frac{y_i}{h} = \frac{1}{2}\left\{1 + \frac{\tanh\left[\alpha_1(i/i_{max} - \frac{1}{2})\right]}{\tanh(\alpha_1/2)}\right\} \; i = 0, 1, 2, \ldots, i_{max} \tag{19}$$

where α_1 is given by $\alpha_2 = \alpha_1/\sinh(\alpha_1)$. After extensive numerical testing, α_2 is taken as 1.5×10^{-3}, which gives $\alpha_1 = 6.811$, to ensure that at least 8 to 10 points lie between the wall and the location of maximum velocity. In the x-direction, extra points (10 points) are added at the location of the heat source ($x_s \le x \le x_s + l_s$). In order to ensure numerical accuracy of the results the computational mesh is refined from 60 × 60 (with 40 × 40 points inside the room) to 120 × 120 (with 80 × 80 inside the room).

The time evolution in the open cavity in the presence of stable thermal stratification is dominated by Brunt-Vaisala time scale $t_b = \frac{h^2}{\alpha}(SGrPr^2)^{-1/2}$ and determines the maximum time step that gives a stable numerical solution. This time step limitation has also been reported by Jones[20], Thompson *et al.*[21] and Henkes[22] in their study of buoyancy-driven turbulent flow in a rectangular cavity. For most of the cases a time step Δt = 1/20 or 1/10 is used to ensure stable numerical solutions for the Grashof numbers considered in this study.

In a partially open enclosure, the difficulties encountered in specifying numerically the appropriate boundary conditions at the outflow are well documented[23-25]. The approach followed in the present work is based on the use of an extended computational domain outside the opening. It was first given by Kettleborough[26]. The outflow boundary conditions are applied at some distance sufficiently far away from the opening such that a further increase does not significantly alter the results obtained for the flow in the enclosure. The dimensions needed for such an

extension beyond the opening are determined numerically. In this work, it was found that an extended computational domain of twice the height of the cavity was sufficient to produce an error of less than 0.1 per cent for the mass outflow rate.

The wall vorticity is a very important quantity and it is produced mainly at no-slip walls and then later advected and diffused into the rest of the flow. The wall vorticity boundary conditions are derived from the non-slip conditions[27]. A first-order finite-difference form is used to approximate the wall vorticity ζ_w as:

$$\zeta_w = -2\frac{\psi_{w+1} - \psi_w}{\Delta n^2} + O(\Delta n). \tag{20}$$

Here, n is the direction normal to wall. The higher-order forms suffer from instability at high Grashof numbers. However, the first-order form is found to be the safest form to use and gave results essentially equal to the higher-order forms. For this reason, the first-order form of the wall vorticity has been used throughout the calculations for the present work.

Initially, the cavity and the surrounding environment are considered to be isothermal and quiescent. After the onset of the heat input in the cavity, the environment at the far end of the computational domain ($X = X_{max}$) is assumed to remain isothermal. The initial conditions for equations (5) and (6) can be obtained from non-zero perturbations in K and ε. Typical value of K_0 is 10^{-6}, ν_t^* is in the range from 2 to 10 and ε_0 is evaluated as $Gr^{1/2}C_\mu K_0^2/(\nu_t^*)_0$. The values of K_0 and $(\nu_t^*)_0$ were varied and were found to have a negligible effect on the computed results at these values.

RESULTS AND DISCUSSION

The computed steady-state flow and thermal fields in a partially open cavity with a heat source located at the middle of the bottom boundary for various opening heights are examined in this section. To illustrate the effect of opening height on the flow, the following three cases are considered:

- Case A with $H_0 = 0.8$
- Case B with $H_0 = 0.5$
- Case C with $H_0 = 0.3$

For each case under consideration, the opening height, and the strength of the heat source, which is represented by the Grashof number, are varied over a wide range (i.e. 10^8-10^{15}). As pointed out earlier, it is very difficult to simulate case C ($H_0 = 0.3$) for $Gr > 10^{11}$, because of the strong thermal stratification generated inside the cavity. Oscillations develop and make the achievement of steady state very difficult. These oscillations are due to internal gravity waves, and this was discussed in greater detail by Abib & Jaluria[3,28].

To view qualitatively the effect of opening height on the flow and on the thermal field, contour plots of the stream function, the temperature and the turbulence quantities are presented. This is followed by a detailed discussion of the mean velocity, temperature, turbulent kinetic energy and turbulent eddy diffusivity profiles. Other variables of interest, such as heat transfer and mass flow rates, hot-cold interface height, and stratification level are also given to highlight the effects of opening height on the flow in a partially open cavity. The results for $Gr = 10^{12}$ are used as an example, since other values of Gr indicate similar trends. However, when differences arise due to a variation in Gr, these are pointed out.

Flow and thermal fields

The steady-state flow and the corresponding thermal fields for a cavity with various opening heights are shown in Figures 2-4, corresponding to the opening height of $H_0 = 0.8$, 0.5, and 0.3 respectively. In these figures the isotherms are presented in the top graph (a), while the

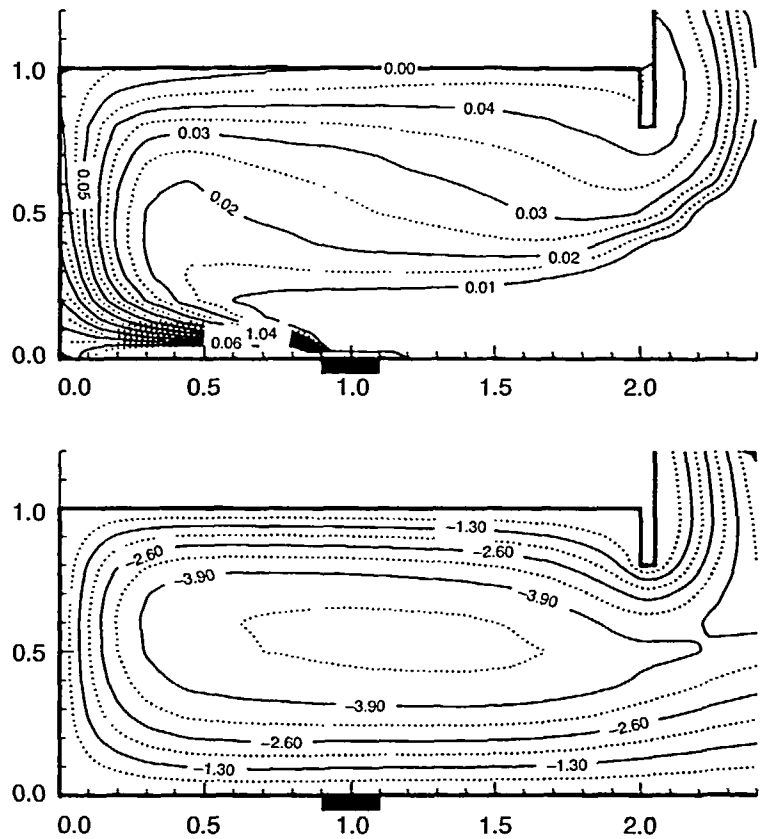

Figure 2 Case A: steady-state turbulent flow and thermal fluid, at $Gr = 10^{12}$, in a partially open cavity with opening height $H_0 = 0.8$. (a) isotherms and (b) streamlines

streamlines are presented in the bottom graph (b). (In order to plot legible labels on the graphs temperature contours are scaled by a factor of 100 and stream function by a factor of 1,000).

Cases A and B (with opening height of 0.8 and 0.5 respectively) have similar flow patterns as shown in Figure 2(b) and Figure 3(b). The only difference is that the flow is more vigorous in case A, because a larger opening is less restrictive to the flow. The flow field reveals the presence of a strong cold floor jet, a hot ceiling jet, and a recirculation region in the middle. The recirculation region is found to increase in size as the opening height is decreased. For a full opening ($H_0 = 1$), a recirculation region does not arise in the cavity.

The isotherms for cases A and B have also a similar pattern as indicated in Figure 2(a) and Figure 3(a). However, the temperature level in case B ($H_0 = 0.5$) is much higher owing to the larger volume of fluid entrapped in the top region of the cavity. In both cases the walls and the ceiling heat up and the surface temperatures rise until a steady state is reached. This temperature rise of the back wall causes a pressure imbalance between the cavity and surrounding ambient medium outside the opening, which forces the vertically rising fire plume to be drawn towards the wall. This phenomenon is the natural convection equivalent of the coanda effect[29] and has received a considerable attention in recent years[30,31]. Despite the coanda effect, the opening size has no significant influence on the trajectory of the plume.

A completely different flow pattern is observed in case C ($H_0 = 0.3$) as shown in Figure 4. Because of a smaller opening size, there is a larger volume of fluid trapped in the upper part of the

cavity, which extends all the way to the door soffit. This upper region or layer becomes stably stratified and almost stagnant. The streamlines in Figure 4(b) show that the fire plume penetrates into this large stably stratified upper layer up to a certain height. As the local buoyancy of the fire plume decreases, the flow stagnates and then turns away to the right towards the opening. The penetration takes place in the form of a horizontal flow in the lower part of the stable upper layer. Because of the stratified layer at the upper region of the cavity, the hot-cold interface Z_i is lowered.

The isotherms in Figure 4(a) also show that the upper layer, generated as a result of the heating, is linearly stratified. This stratification is stable because the temperature increases with height and, as a consequence, the turbulence in the upper layer decays and the flow becomes laminar. This is an example of a circumstance where thermal stratification is generated within the cavity as a result of the interaction between the cavity and the ambient medium outside the opening.

The Mean velocity and temperature

The mean velocity profiles are shown in Figure 5. The graph shows the U component variation with Y at several different X locations, at $Gr = 1 \times 10^{12}$, for the three cases: A, B, and C. Again, the mean velocity profiles show that the cases A and B have a similar flow pattern. The flow in case A is slightly more vigorous than that for case B. However, case C is quite different. In Figure 5, for instance, in case A ($H_0 = 0.8$) the maximum velocity is attained at the opening, $X = 2.0$, because

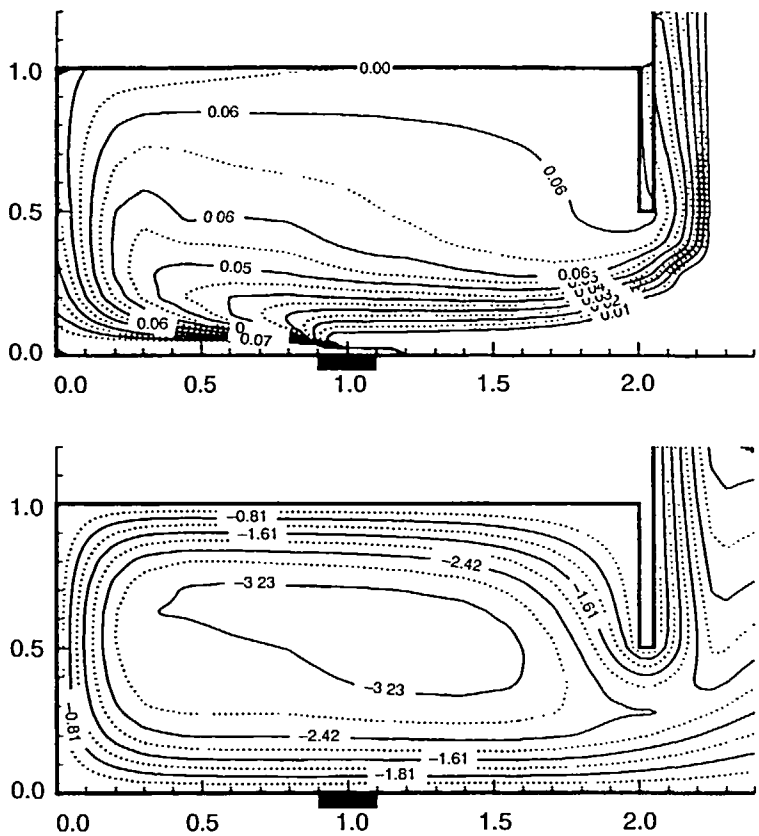

Figure 3 Case B: steady-state turbulent flow and thermal field, at $Gr = 10^{12}$, in a partially open cavity with opening height $H_0 = 0.5$. (a) isotherms and (b) streamlines

the flow is essentially unobstructed. However, in case C ($H_0 = 0.3$) the maximum velocity is not attained at the opening but at a location between the heat source and the back wall. The figure also shows that, in case C, the upper layer is stagnant with the maximum penetration distance of the fire plume δp equal to 0.55. The penetration distance δp is computed as the maximum vertical distance from the floor to the location where the horizontal component of the velocity u in the top part of the main (lower) cell becomes zero.

The vertical distribution of the mean temperature is shown in Figure 6 for the same three cases, at $Gr = 1 \times 10^{12}$. The figure shows that the mean temperature level rises as the opening height is decreased because of the hot fluid entrapped in the upper region of the cavity. Furthermore, when the opening height is decreased below 0.5, because of entrapped fluid in the upper region, an essentially linear stratification is generated.

Based on the temperature distribution, the cavity can be considered to be divided into a hotter upper layer and cooler lower layer. From plots of the temperature variation along the vertical direction, the height of the hot-cold interface Z_i can be quantitatively determined. Following Steckler *et al.*[7] the height of the interface is estimated from the temperature profile data as the position of rapid temperature change between the lower and the upper portions of the cavity. These temperature profiles illustrate how diffusion and mixing preclude a sharp designation of Z_i. Consequently, the interface height could only be determined to within ±10-25 per cent accuracy. This interface estimation technique was also used by others[32,33].

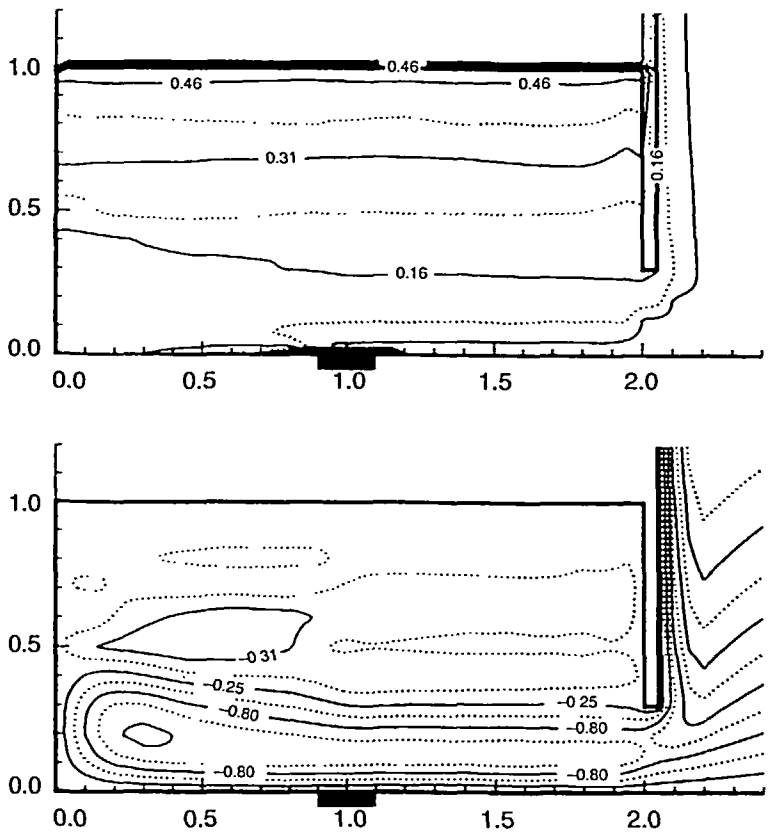

Figure 4 Case C: steady-state turbulent flow and thermal field, at $Gr = 10^{12}$, in a partially open cavity with opening height $H_0 = 0.3$. (a) isotherms and (b) streamlines

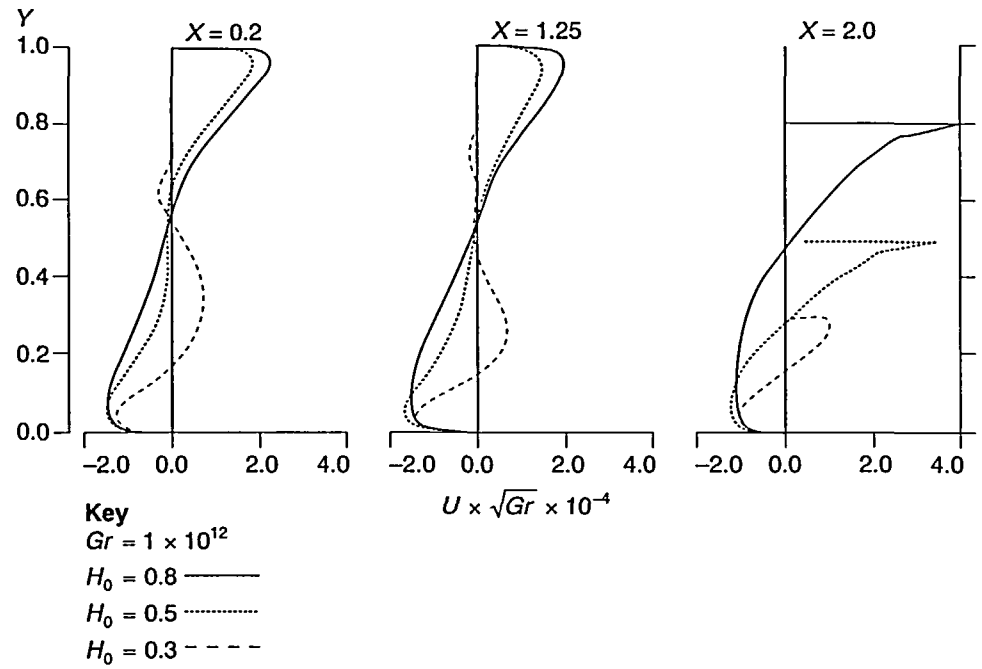

Figure 5 Horizontal component of the mean velocity U as function of the vertical distance Y, in a partially open cavity with various opening heights, at $Gr = 10^{12}$

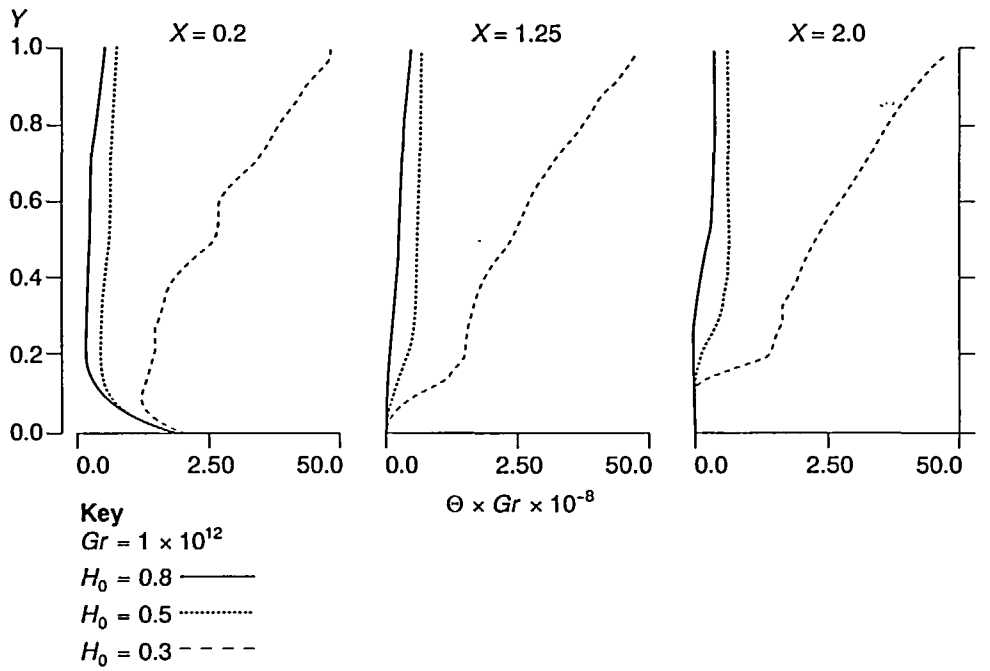

Figure 6 Vertical distribution of the mean temperature θ in a partially open cavity with various opening heights, at $Gr = 10^{12}$

Table 2 Variation of the penetration distance δp, the height of the hot-cold interface Z_i, and the stratification level γ with the opening height H_0, at $Gr = 10^{12}$

	H_0		
	0.3	0.5	0.8
δp	0.4	1.0	1.0
Z_i	0.4-0.15	0.5-0.3	0.6-0.5
γ	0.625	0.26	0.2-0.1

The height of the interface varies slightly along the x-direction. To study the effect of the opening size on the location of the interface, the horizontal location is fixed (i.e. for instance the mid-cavity). The interface Z_i is given in Table 2 as function of the opening height H_0. It is seen that, as the opening height is decreased, the temperature level increases, indicating a significant lowering of the hot-cold interface. This implies that the hot fluid is recirculated and returns towards the heated area. This result is consistent with the experimental observations of McCaffrey and Quintiere[11]. The lowering of the hot-cold interface has another implication regarding safety. This means that the hot combustion gases and the smoke layer are closer to floor and could prevent, or curb, the fire-fighting and rescue operations.

Turbulent quantities

The turbulent quantities such the turbulent kinetic energy (hereafter referred to as TKE) K and the turbulent eddy diffusivity ν_t/ν distributions, at $Gr = 10^{12}$, are shown in Figures 7-9. Again, both K and ν_t/ν contours show a similar pattern for the opening heights of cases A and B. Most of the turbulence is generated in the fire plume which becomes attached to the back wall, due to imbalance of pressure between the cavity and the ambient medium[31], and in the shear layer where the cold inflow and the hot outflow meet. At both of these locations, turbulence production by shear is dominant over that due to buoyancy. Since the temperature gradient is positive, buoyancy production (defined in equation (8)) is a sink term. In the ceiling area, turbulence is convected by the ceiling jet and, therefore, both K and ν_t/ν have high values. In mid-cavity, the velocities are low and there is a stable temperature stratification (see Figures 5-6).

Since the destruction of turbulence by stable gradient depends on the ratio of turbulence destruction due to stratification to turbulence production by shear, this will result in reduction of turbulence and, hence, both K and ν_t/ν have a low value (cases A and B). The locations of the maximum square root of the TKE, $K_{max}^{1/2} \times Gr^{1/2}$, for cases A and B, are close to the doorway soffit (see Table 3). This corresponds to the the location of maximum velocity. From the table, it is observed that this location does not vary with Gr. This is expected physically because, at any given heat input, the location of the maximum velocity is at the doorway soffit where the flow rushes to leave the enclosure.

In case C ($H_0 = 0.3$), the trends are quite different. Turbulence is generated in the fire plume and the shear layer at the opening. It is convected and diffused throughout the cavity by the re-circulating flow. Because of the presence of the strong stable temperature gradient in the upper layer of the cavity, the turbulence that is convected in the upper layer is destroyed by this stable gradient. As a result, the flow in the upper layer is relaminarized and turbulence is confined to locations such as the shear layers at the lower left corner (fire plume attachment to the back wall) and outside the opening (the hot rising wall plume). Unlike the previous cases, A and B, the location of maximum square root of the TKE for case C is near the floor between the source and back wall. As Gr is increased, the location of $K_{max}^{1/2}$ shifts towards the back wall. The rise of the fire plume above the source is inhibited by the existence of the stratified upper layer. Therefore, the fire plume never reaches the ceiling since there is not enough buoyancy to drive it upwards. As a consequence, the maximum velocity does not occur at the exit plane but somewhere between the source and back wall.

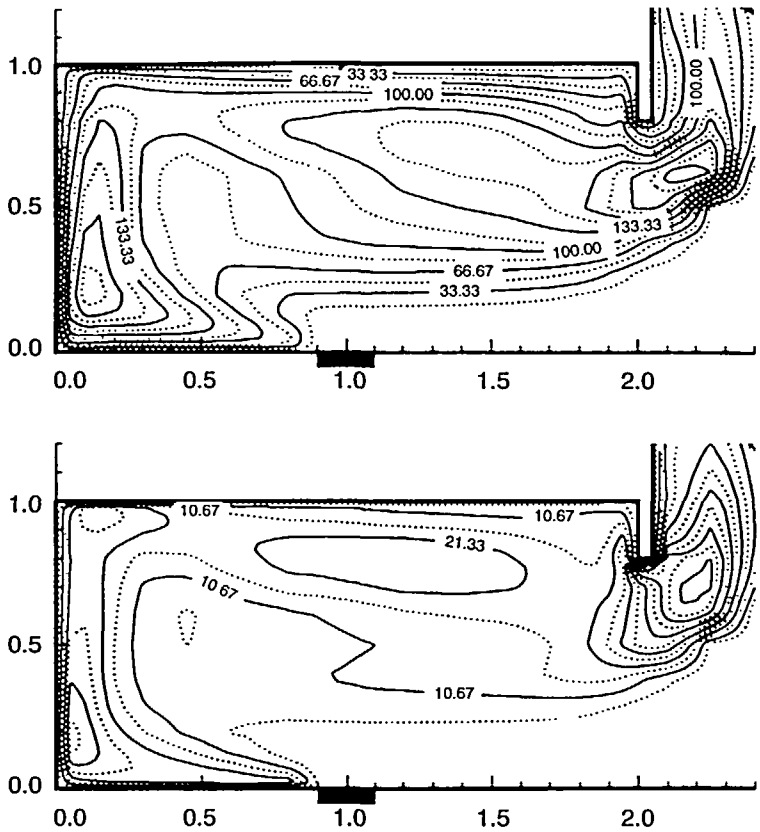

Figure 7 Case A: contour lines of (a) the turbulent kinetic energy K and (b) the turbulent eddy diffusivity ν_t/ν, at $Gr = 10^{12}$, in a partially open cavity with opening height $H_0 = 0.8$

The cases considered so far are with $Gr = 10^{12}$. It is sufficient to say that similar trends exist for other values of Gr. Of course the flow is more vigorous as Gr is increased and, hence, the turbulence level is higher.

Turbulent fluctuations and eddy diffusivity profiles

Profiles of square root of the TKE $K^{1/2}$ and of the eddy diffusivity ν_t/ν at $Gr = 10^{12}$, are shown in Figures 10 and 11. Figure 10 corresponds to the case A ($H_0 = 0.8$), and shows two peaks in $K^{1/2}$ and ν_t/ν, one near the boundary layer at the back wall and the other at the soffit wall. The maximum values of $K^{1/2}$ and ν_t/ν are located near the exit at the height of the soffit.

Figure 11 corresponds to case C ($H_0 = 0.3$) and, as explained earlier, shows a trend quite different from the previous case. In Figure 11, there is only one peak in both $K^{1/2}$ and ν_t/ν profiles and these are located at the boundary layer near the back wall. Both $K^{1/2}$ and ν_t/ν also decrease along the vertical direction due to the presence of the stable stratified layer in the upper part of the cavity. This disappearance of the second peak at the soffit wall is due to the inability of the fire plume to penetrate into the upper layer and form a ceiling jet as in the case where the ambient medium is not stably stratified[2].

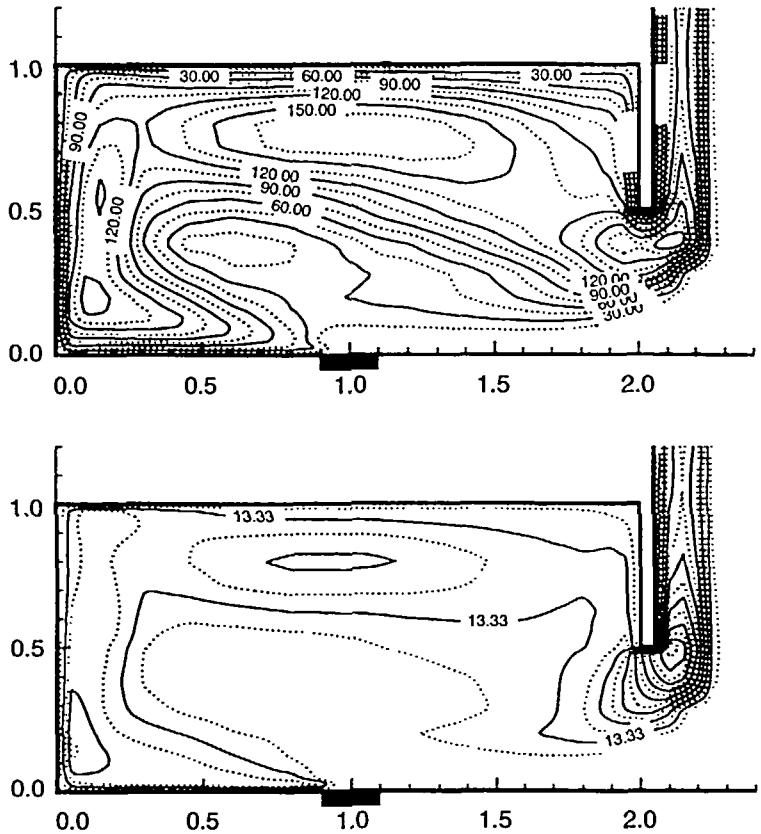

Figure 8 Case B: contour lines of (a) the turbulent kinetic energy K and (b) the turbulent eddy diffusivity ν_t/ν, at $Gr = 10^{12}$, in a partially open cavity with opening height $H_0 = 0.5$

Mass outflow and heat transfer rates

The heat transfer rate at the source surface, in terms of a Nusselt number defined as

$$\overline{Nu} = \frac{\bar{h}h}{\kappa} = \frac{1}{{L_s}^2}\int_0^{L_s}\frac{1}{\Theta_s}dX \tag{21}$$

and the mass outflow rate, are two important engineering output variables. The Nusselt number characterizes the surface temperature level or the energy loss/gain at the surface depending on the nature of the boundary conditions. The mass outflow rate is an indication of the amount of ventilation in the enclosure. The effect of opening height on the mass outflow rate and the heat transfer rate for turbulent flow in a partially open cavity, is examined. These results are compared with the available experimental data in the literature.

The mass outflow rate versus Gr is plotted in Figure 12 for different opening heights. It shows an increasing flow rate with Gr and with the opening height H_0. A least squares curve fit is performed on the numerical data and the following correlation is obtained for mass outflow rate as function of Gr and opening height H_0,

$$\dot{m}\sqrt{Gr} = 0.211\, {H_0}^{1.21}\, {Gr}^{0.36}. \tag{22}$$

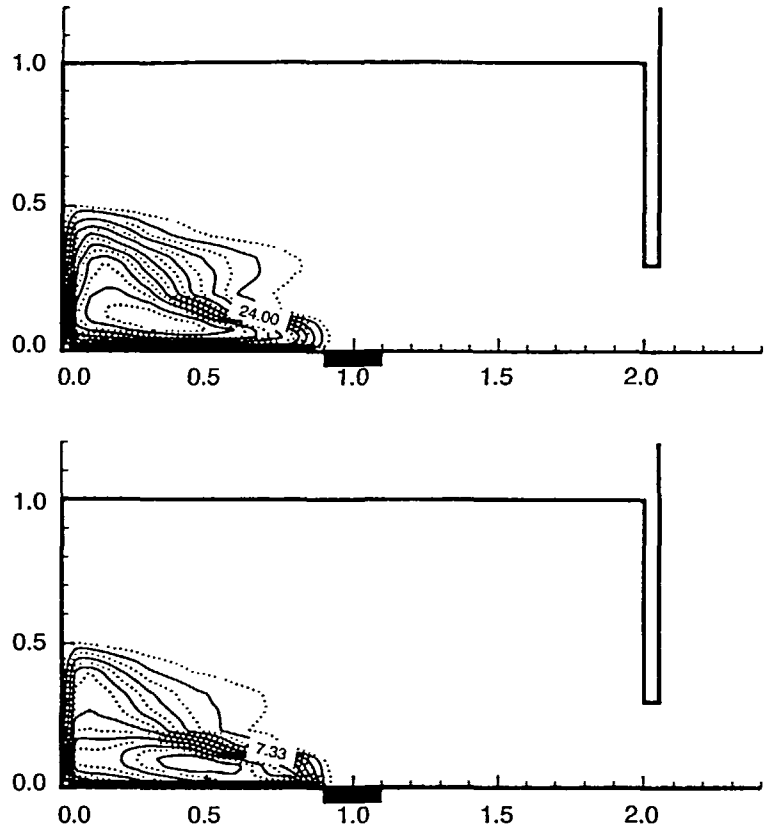

Figure 9 Case C: contour lines of (a) the turbulent kinetic energy K and (b) the turbulent eddy diffusivity ν_t/ν, at $Gr = 10^{12}$, in a partially open cavity with opening height $H_0 = 0.3$

The range over which the above correlation is valid is $10^8 \leq Gr \leq 10^{15}$ and $0.3 \leq H_0 \leq 1.0$. It includes both laminar and turbulent flow regimes. The computed mass outflow rate at the opening computed by Satoh *et al.*[34] is given as

Table 3 Variation of maximum square root of the TKE, $K_{max}^{1/2} \times Gr^{1/2}$ with opening height H_0

H_0	Gr 10^9	10^{10}	10^{11}	10^{12}	10^{13}	10^{14}	10^{15}
	166.02	1,114.14	2,773.81	5,386.09	8,601.3	–	–
0.3	$X = 1.99$	0.799	$X = 0.608$	$X = 0.441$	$X = 0.441$		
	$Y = 0.134$	0.022	$Y = 0.088$	$Y = 0.088$	$Y = 0.08$		
	–	1,322.5	4,291.5	9,264.39	13,936.3	–	–
0.5		$X = 1.99$	$X = 1.99$	$X = 1.99$	$X = 1.99$		
		$Y = 0.386$	$Y = 0.478$	$Y = 0.479$	$Y = 0.497$		
	–	1,680.18	5,409.25	13,235.2	18,606.5	33,318.2	86,313.4
0.8		$X = 1.996$	$X = 1.998$	$X = 1.998$	$X = 1.999$	$X = 1.986$	$X = 1.986$
		$Y = 0.797$	$Y = 0.797$	$Y = 0.797$	$Y = 0.797$	$Y = 0.797$	$Y = 0.816$

$$\dot{m}\sqrt{Gr} \propto H_0^{1.28}\, Gr^{1/3}. \tag{23}$$

Steckler *et. al.*[7] give the mass rate as a function of the opening height H_0 as

$$\dot{m}\sqrt{Gr} \propto W\, H_0^{1.5} \tag{24}$$

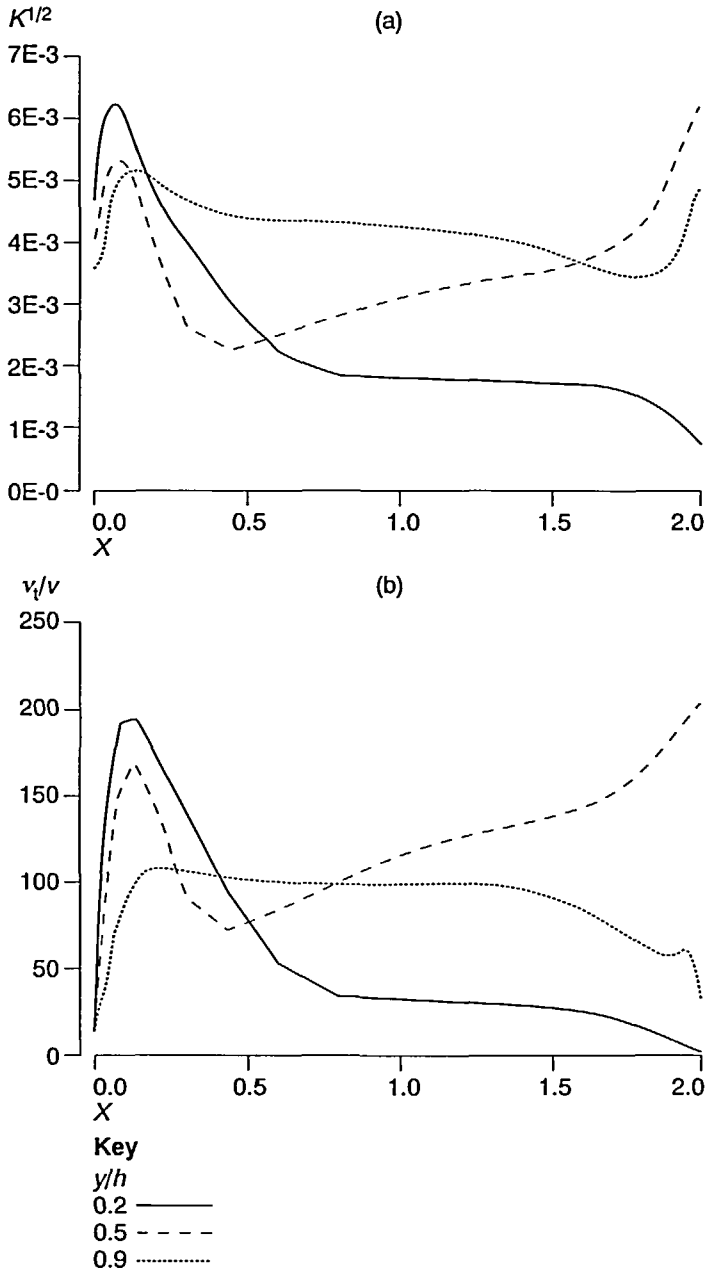

Figure 10 (a) The velocity fluctuation $K^{1/2}$ and (b) the turbulent eddy diffusivity ν_t/ν profiles, at $Gr = 10^{12}$, for a partially open cavity with an opening height $H_0 = 0.8$.

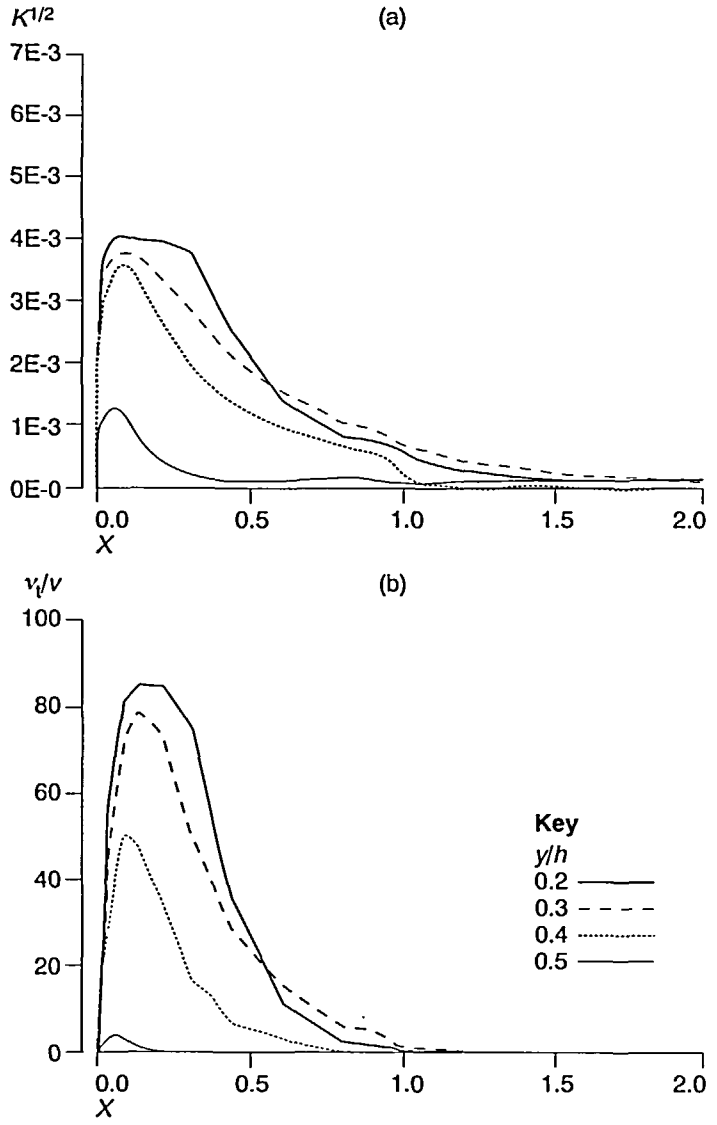

Figure 11 (a) The velocity fluctuation $K^{1/2}$ and (b) the turbulent eddy diffusivity ν_t/ν profiles, at $Gr = 10^{12}$, for a partially open cavity with an opening height $H_0 = 0.3$.

where W is the width of the opening. Despite the disparity among the various results presented, the experimental results of Satoh[35] for a doorway opening is in fairly good agreement with the present result.

The average heat transfer rate at the source $\overline{Nu}_s$ versus Gr is plotted in Figure 13 for various opening heights. The figure shows that the curves which correspond to different opening heights collapse into a single curve. This indicates the insensitivity of $\overline{Nu}_s$ to the variation in the opening height at higher Gr. This occurs because the flow and the heat transfer are very vigorous and, therefore, the effect due to the variation in the opening size is negligible in comparison to the effects due to an increase in the heat input.

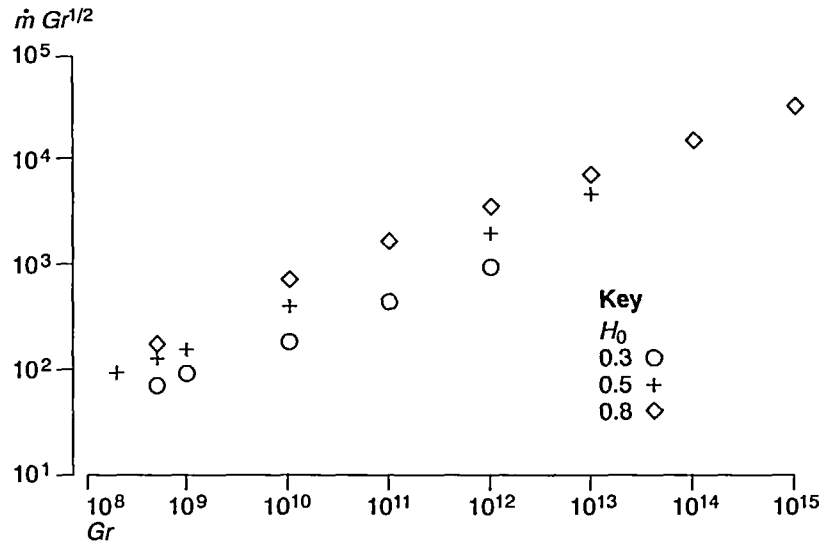

Figure 12 Average mass outflow rate $\dot{m} \times Gr^{1/2}$ versus Gr for a partially open cavity with different opening heights

Maximum velocity in the ceiling jet

The maximum horizontal velocity U_{max} in the ceiling jet versus Gr is also plotted in Figure 14 for various opening heights. This velocity is seen to increase with Gr as the flow becomes more intense due to an increase in the heat input. A least squares curve fit is performed for U in the ceiling jet, yielding the following correlation:

$$U_{max} = 0.623 H_0^{1.5} Gr^{0.39}, \quad 10^4 \le Gr \le 2 \times 10^8 \tag{25}$$

$$U_{max} = 1.426 H_0^{0.6} Gr^{0.36}, \quad 2 \times 10^8 \le Gr \le 10^{15} \tag{26}$$

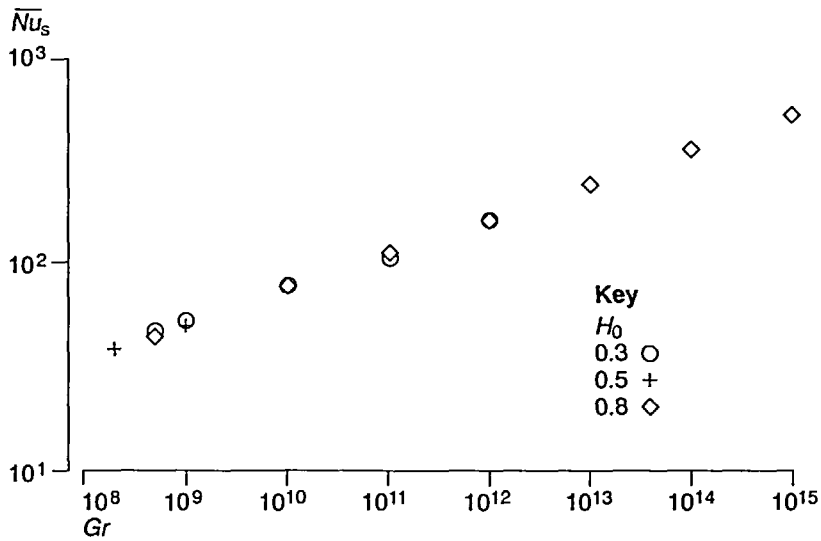

Figure 13 Average Nusselt number $\overline{Nu}_s$ versus Gr for a partially open cavity with different opening heights

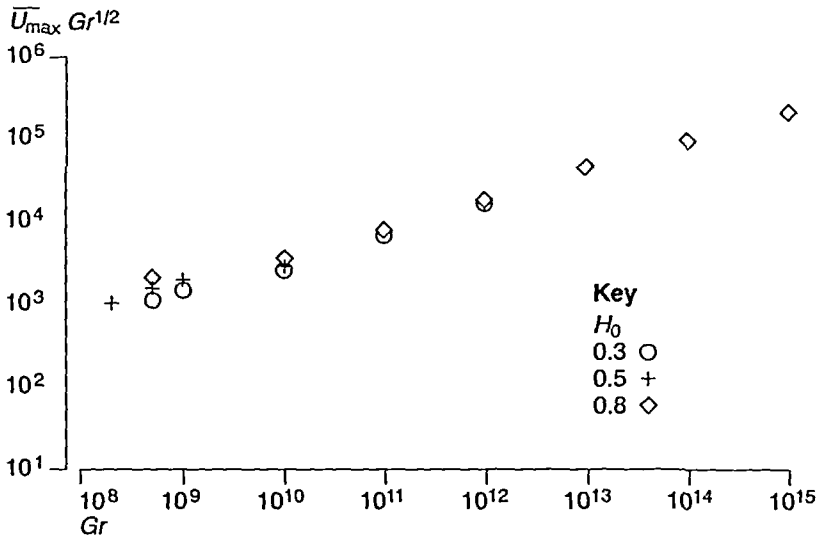

Figure 14 Maximum mean velocity $U_{max} \times Gr^{1/2}$ versus Gr in a partially open cavity with different opening heights

These equations show that, for higher Gr, the ceiling jet is a strong function of Gr and a weak function of the opening height. Regarding the Gr dependence, the experimental work of McCaffrey and Quintiere[11] reported U_{max} (in the ceiling jet) to be:

$$U_{max} \propto Gr^{1/2}, \tag{27}$$

while in the present work, U_{max} is found to vary as:

$$U_{max} \propto Gr^{0.36}. \tag{28}$$

Alpert's[36] analytical results of an unobstructed ceiling jet yields $U_{max} \propto Gr^{1/3}$. This discrepancy is suspected to be due to 3D and thermal radiation effects which are neglected in the present work.

Stratification level, penetration distance, and interface location

First, attention is focused on the thermal stratification that is generated within the cavity at large Gr as the opening height is varied. The in-room stratification level γ is obtained by first horizontally averaging the vertical temperature profiles and then taking the slope of the resulting profile which is seen to decrease as the opening height is increased. Table 2 shows the effect of the opening height on the stratification level. At high Gr (say $Gr = 10^{12}$) a stratified upper layer is formed. The depth of this layer increases as the opening height is reduced. For $H_0 = 0.8$ and 0.5, we have an almost linearly stratified upper layer. The fire plume rises above the source, gets attached to the back wall and then may or may not reach the ceiling depending on thermal stratification generated for the given opening height. Table 2 also shows the penetration distance of the fire plume. It is clear that, in cases A and B, the fire plume does reach the ceiling. However, for case C, the plume fails to reach the ceiling because of the strong thermal stratification ($\gamma = 0.65$) that is generated within the cavity. The penetration height δp is 0.4 at $Gr = 10^{12}$.

The effect of the opening height on the location of the hot-cold interface Z_i is also given for this case. The location of the interface varies horizontally and so the maximum and the minimum values are also given in Table 2. The maximum value of Z_i occurs near the back wall where the fire plume has penetrated the most in the upper layer. The minimum value of Z_i occurs at the door

Table 4 Variation of the penetration distance δp, the height of the hot-cold interface Z_i, and the stratification level γ with Gr in a partially open cavity with $H_0 = 0.3$

	Gr			
	10^9	10^{10}	10^{11}	10^{12}
δp	1.0	0.7	0.5	0.4
Z_i	0.5-0.4	0.2-0.15	0.4-0.2	0.4-0.15
γ	0.0	0.35	0.61	0.625

opening where the cold inflow and the hot outflow meet. As seen earlier, case C ($H_0 = 0.3$) is quite different from the two other cases (A and B). This is because of the large linearly stratified layer generated in the top part of the cavity for this case.

Next, the effects of Gr on the stratification level, penetration distance of the fire plume and the location of the hot-cold interface for case C (with an opening height of $H_0 = 0.3$) is considered. The results are summarized in Table 4. At $Gr = 10^9$, the plume is able to reach the ceiling. Because of mixing due to turbulence and recirculation, a uniform temperature is established in the upper-layer. The stratification level is, therefore, close to zero and the hot-cold interface height Z_i assumes its highest value for case C ($Z_i = 0.7$). As Gr is increased to $Gr = 10^{10}$ the wall plume is unable to reach the ceiling (penetration distance $\delta p = 0.7$) due to the stronger stratification that is generated in the upper-layer ($\gamma = 0.33$). As a result, turbulence is reduced, resulting in less mixing. Because the penetration distance is now decreased, the location of the interface drops downward. As Gr is further increased to 10^{11}-10^{12}, the thermal stratification level increases to 0.61-0.625 because of the generation of a large stagnant region at the top of the cavity. As a result, the penetration distance and the height of the interface are both found to decrease.

CONCLUSIONS

A numerical study of the two-dimensional turbulent penetrative and recirculating flow induced by localized heating at the bottom surface of a partially open rectangular cavity is carried out. The background ambient medium is taken as isothermal. The study focuses on the internally generated thermal stratification within the cavity. It is found that thermal stratification can be generated within the partially open cavity, at high Gr, for relatively small opening heights, in particular, for doorway openings. The height of the generated stratified layer and the corresponding stratification level are expected to increase, at a given Gr, when the opening height is decreased. Therefore, a behaviour similar to that for stable ambient stratification cases is found to arise. This behaviour includes the lowering of the interface Z_i between the hot gases and the cold lower region, failure of the fire plume to penetrate into the stably stratified upper layer generated within the cavity, and decay of turbulence due to the strong stable thermal stratification, and hence, the relaminarization of the flow in the upper layer of the cavity.

In addition, as the opening height is reduced, the thermal stratification that arises as a result of the fire in the cavity reduces the buoyancy level and, hence, results in lower velocities and smaller mass outflow rates. However, the Nusselt number for heat transfer from the source is seen to be affected to a small extent by the variation of the opening height. Comparison with experimental results show a good agreement for the thermal field, but there is some discrepancy in the velocity field. This difference may be due to three-dimensional effects which the present study does not take into account.

ACKNOWLEDGEMENTS

The authors acknowledge the partial support provided by the Building and Fire Research Laboratory, National Institute of Standards and Technology, under Grant No. 60NANB1H1171 for this work.

REFERENCES

1 Quintiere, J.G., Growth of fire in building compartments, in *Fire Standards and Safety*, Robertson, A.F. (Ed.), American Society for Testing and Materials, *ASTM STP 614*, 131-167 (1977)
2 Quintiere, J.G., Perspective on compartment fire growth, *Combust. Sci. Technol*, **39**, 11-54 (1984)
3 Abib, A.H. and Jaluria, Y., Turbulent penetrative and recirculating flow in a compartment fire, *J. Heat Transfer*, **117**, 927-955 (1995)
4 Kawagoe, K., Fire behaviour in rooms, *Rep. 27*, Building Research Institute, Japan (1958)
5 Ku, A.C., Doria, M.L. and Lloyd, J.R., Numerical modeling of buoyant flows generated by fire in a corridor, *Proc. 16th Symp. (int.) on Combustion*, Combustion Institute, 1372-1384 (1976)
6 Emmons, H.W., The prediction of fire in buildings, *17th Symp. (int.) Combustion*, Combustion Institute, Pittsburgh, **117**, 927-985 PA, 1101 (1978)
7 Steckler, K.D., Quintiere, J.G. and Rinkinen, W.J., Flow induced by fire in a compartment, *19th Symp. (Int.) Combustion*, Combustion Institute, 913-920 (1982)
8 Markatos, N.C., Malin, M.R., and Cox, G., Mathematical modeling of buoyancy-induced smoke flow in enclosures, *Int. J. Heat Mass Transfer*, **25**, 63-75 (1982)
9 Satoh, K., Lloyd, J.R., Yang, K.T. and Kanury, A.M., A numerical finite-difference study of the oscillatory behaviour of vertically vented compartments, in Shih, T.M. (Ed.), *Numerical Properties and Methodologies in Heat Transfer*, Hemisphere Publishing Corp., New York, 517-528 (1983)
10 Simcox, S., Wilkes, N.S. and Jones, I.P., Computer simulation of the flow of hot gases from the fire at King's Cross underground station, *Proc. Symp. King's Cross Underground Fire*, Inst. Mech. Eng, London (1989), 19-25.
11 McCaffrey, B.J. and Quintiere, J.G., Buoyancy driven countercurrent flow generated by a fire source, in Spalding, D.B. and Afgan, N. (Eds.), *Heat Transfer and Turbulent Buoyant Convection*, Vol. II, Hemisphere Publishing Corp., New York, 457-472 (1977)
12 Quintiere, J.G., An approach to modelling wall fire spread in a room, *Fire Safety Journal*, **3**, 201-214 (1981)
13 Lam, C.K.G. and Bremhorst, K., A modified form of the $k-\varepsilon$ model for predicting wall turbulence, *J. Fluid Engng*, **13**, 456-460 (1981)
14 Davidson, L., Calculation of the turbulent buoyancy-driven flow in a rectangular cavity using an efficient solver and two different low Reynolds $k-\varepsilon$ turbulence models, *Numerical Heat Transfer*, Part A, **18**, pp. 129-147 (1990)
15 Launder, B.E. and Spalding, D.B., The numerical computation of turbulent flows, *Comput. Meth. Appl. Mech. Eng.*, **3**, 269-289 (1974)
16 Rodi, W., Turbulence models and their application in hydraulics, a state of the art review, *International Association for Hydraulics Research*, Delft, The Netherlands (1980)
17 Fraikin, M.P., Portier, J.J. and Fraikin, C.J., Application of a $k-\varepsilon$ turbulence model to an enclosed buoyancy driven recirculating flow, *ASME-AIChE Nat. Heat Transfer Conference*, Paper No. 80-HT-68 (1980)
18 Patankar, S.V., *Numerical Heat Transfer and Fluid Flow*, Hemisphere Publishing Corp., Washington, DC (1980)
19 Abib, A.H., Penetrative and recirculating flows in enclosures with openings, PhD Thesis, Rutgers – The State University of New Jersey, New Brunswick, NJ (1992)
20 Jones, I.P., The convergence of a simple iterative strategy for strongly stratified flows, in Taylor, C. (Ed.), *Numer. Meth. on Laminar and Turbulent Flow*, Pineridge Press, Swansea, 733-740 (1985)
21 Thompson, C.P., Wilkes, N.S. and Jones, I.P., Numerical studies of buoyancy-driven turbulent flow in a rectangular cavity, *Int. J. Num. Meth. Engng.*, **24**, 89-99 (1987)
22 Henkes, R.A.W.M., Natural convection boundary layers, PhD Thesis, Delft University, Delft, The Netherlands (1990)
23 Le Quere, P., Humphrey, J.A.C. and Sherman, F.S., Numerical calculation of thermally driven two-dimensional unsteady laminar flow in cavities of rectangular cross section, *Numerical Heat Transfer*, **4**, 249-283 (1981)
24 Penot, F., Numerical calculation of two-dimensional natural convection in isothermal open cavities, *Numerical Heat Transfer*, **5**, 421-437 (1982)
25 Chan, Y.L. and Tien, C.L., Numerical study of two-dimensional laminar natural convection in shallow open cavities, *Int. J. Heat and Mass Transfer*, **28**, 603-612 (1985)
26 Kettleborough, C.F., Transient laminar free convection between heated vertical plates including entrance effects, *Int. J. Heat and Mass Transfer*, **15**, 883-896 (1972)
27 Roache, P.J., *Computational Fluid Dynamics*, Hermosa Publishers, Albuquerque, New Mexico, (1972)
28 Abib, A.H. and Jaluria, Y., Penetrative convection in a stably stratified enclosure, *Int. J. Heat and Mass Transfer*, **38**, 2489-2500 (1995)
29 Reba, I., Application of the coanda effect, *Scientific American*, **214**, 6, 84-92 (1966)

30 Pera, L. and Gebhart, B., Laminar plume interactions, *J. Fluid Mech.*, **68**, 259-271 (1975)
31 Agrawal, R. and Jaluria, Y., Deflection of a two-dimensional natural convection wake due to the presence of a vertical surface in close proximity, *J. Fluid Mech.*, **201**, 35-56 (1989)
32 Goldman, D. and Jaluria, Y., Effect of opposing buoyancy on the flow in free and wall jet, *J. Fluid Mech.*, **166**, 41-56 (1986)
33 Kapoor, K. and Jaluria, Y., Penetrative convection of a plane turbulent wall jet in a two-layer thermally stable environment, *Int. J. Heat Mass Transfer*, **36**, 155 (1993)
34 Satoh, K., Lloyd, J.R. and Yang, T.K., A numerical study of a buoyant flow in enclosures with vertical openings – effect of heat source and opening locations, *ASME Nat. Heat Transfer Conf.*, Buffalo, NY (1984)
35 Satoh, K., An approach to modeling of aircraft cabin fire phenomena – the ventilation effect of location and geometry of the heat source and opening in an aircraft passenger cabin, *Report of Fire Research Institute*, Japan, No. 53, 43 (1982)
36 Alpert, R.L., Fire induced turbulent ceiling jet, *FMRC Serial No. 197722-2*, Factory Mutual Research Corp., Norwood, MA (1971)